

Innate extracellular mouse Hsp70 inflammatory properties are mediated by the interaction of Siglec-E and LOX-1 receptors

Thiago J. Borges^{1,*}  · Karina Lima^{1,2}  · Ayesha Murshid³ · Isadora T. Lape¹ · Maurício M. Rigo⁴ · Benjamin J. Lang³  · Thais J. Teani⁵  · Shoib S. Siddiqui⁶ · Leonardo V. Riella¹ · Cristina Bonorino² · Stuart K. Calderwood^{3,*} 

Received: 12 March 2025 / Revised: 7 May 2025 / Accepted: 20 May 2025

© 2025 The Author(s). Published by Elsevier Inc. on behalf of Cell Stress Society International. This is an open access article under the CC BY-NC-ND license (<http://creativecommons.org/licenses/by-nc-nd/4.0/>).

Abstract

Innate immune responses to cell damage-associated molecular patterns induce a controlled degree of inflammation, ideally avoiding the promotion of intense unwanted inflammatory adverse events. When released by damaged cells, Hsp70 can stimulate different responses that range from immune activation to immune suppression. The effects of Hsp70 are mediated through innate receptors expressed primarily by myeloid cells, such as dendritic cells (DCs). The regulatory innate receptors that bind to extracellular mouse Hsp70 (mHsp70) are not fully characterized, and neither are their potential interactions with activating innate receptors. Here, we show that extracellular mHsp70 interacts with a receptor complex formed by both inhibitory Siglec-E and activating lectin-like oxidized low-density lipoprotein receptor-1 (LOX-1) on DCs. We also find that this interaction takes place in lipid microdomains within the plasma membrane, and that Siglec-E acts as a negative regulator of LOX-1-mediated innate activation upon mHsp70 or oxidized LDL binding. Thus, Hsp70 can both bind to and modulate the interaction of inhibitory and activating innate receptors on the cell surface. These findings add another dimension of regulatory mechanism to indicate how self-molecules contribute to dampening of exacerbated inflammatory responses.

Keywords Heat shock protein 70 · Siglec-E · Lectin-like oxidized low-density lipoprotein receptor-1 · Innate · Dendritic cells

Abbreviations: APCs, antigen-presenting cells; BMDCs, bone-marrow-derived dendritic cells; DAMPs, damage-associated molecular patterns; DCs, dendritic cells; FEEL-1, fasciclin, EGF-like, laminin-type EGF-like, and link domain-containing scavenger receptor-1; Hsp70, heat shock protein 70; LDL, low-density lipoprotein; LOX-1, lectin-like oxidized low-density lipoprotein receptor-1; oxLDL, oxidized low-density lipoprotein; PRRs, pattern-recognition receptors; Siglec, sialic acid binding Ig-like lectin; SR, scavenger receptors; SREC-I, scavenger receptor expressed by endothelial cells I; Tregs, regulatory T cells

* Thiago J. Borges
tdejesusborges@mgh.harvard.edu

* Stuart K. Calderwood
stukcalderwood@gmail.com

¹ Center for Transplantation Sciences, Department of Surgery, Massachusetts General Hospital, Boston, MA 02129 USA

² Basic Health Sciences Department, Federal University of Health Sciences of Porto Alegre (UFCSA), Porto Alegre, RS, Brazil

³ Department of Radiation Oncology, Beth Israel Deaconess Medical Center, Harvard Medical School, Boston, MA 02215 USA

⁴ Hackensack Meridian Health, Center for Discovery and Innovation, Nutley, NJ 07110, USA

⁵ Hospital Israelita Albert Einstein, São Paulo, SP, Brazil

⁶ School of Life and Medical Sciences, University of Hertfordshire, Hatfield, United Kingdom.

Introduction

A key question in innate immunity is how cells distinguish between self and foreign molecules with high degrees of homology. Innate immune responses are initiated by pattern-recognition receptors, expressed in abundance by macrophages and dendritic cells (DCs). Their ligands vary from pathogen-associated molecular patterns present in microorganisms to damage-associated molecular patterns derived from injured tissues. Ideally, an effector immune response must be able to resolve any infection or sterile trauma with no exacerbating deleterious immunopathology. Importantly, the interplay of innate signals will shape the adaptive immune responses that ensue.¹

The heat shock protein (HSP) 70 is one of the most evolutionarily conserved proteins, but has complex effects when present in the extracellular microenvironment. Mouse HSP70 (mHSP70) binds to scavenger receptors such as lectin-like oxidized low-density lipoprotein receptor-1 (LOX-1), scavenger receptor expressed by endothelial cells I (SREC-I), and fasciclin, EGF-like, laminin-type EGF-like, and link domain-containing scavenger receptor-1 and triggers inflammatory innate immunity in DCs.² DCs are the major antigen-presenting cells (APCs) in mammals and play a crucial role in inducing and regulating the T cell responses that initiate upon engaging MHC:peptide complexes and costimulatory molecules (CD86) expressed by the APCs. Conversely, HSP70 can exhibit anti-inflammatory properties through its modulation of APCs and the induction of regulatory T cells (Tregs).³⁻⁷ Consequently, extracellular HSP can either enhance or suppress immunity depending on the microenvironmental context. Recent findings demonstrated that human HSP70 could interact with paired receptors Siglec-5 and Siglec-14, with Siglec-14 enhancing IL-8 and TNF- α production in human monocytes following stimulation by human HSP70, while Siglec-5 reduced this inflammatory signaling.⁸ However, the mechanism by which HSPs could induce opposing responses in innate immune cells is poorly understood at a molecular level. One possible scenario is that the same HSP70 molecule could be recognized by different functional receptors to activate distinct innate responses. Alternatively, they could be recognized by the same receptor but lead to differential immune responses due to interaction with distinct coreceptors.

Given the importance of murine models for *in vivo* immunological studies, we sought to identify whether a similar Siglec-based mechanism exists for murine responses to mHSP70. Based upon its previously described anti-inflammatory properties, we identified mouse

Siglec-E as a potential candidate by which inflammatory responses to mHSP70 may be regulated. Here, we show that extracellular mHSP70 binds to mouse Siglec-E. Notably, Siglec-E could also interact with the activating mHsp70 receptor LOX-1, forming a complex within lipid microdomains in the plasma membranes of DCs. Deletion of Siglec-E from DCs increased LOX-1-triggered activation, suggesting that Siglec-E restrains LOX-1 engagement on DCs. Our results suggest a mechanism by which innate counter-receptors heterodimerize on the cell surface, forming a receptor complex that binds to nonglycosylated self-molecules, thus contributing to the intricate orchestration of immune responses.

Results

Extracellular mHSP70 interacts with Siglec-E

We first analyzed the potential role of Siglec-E, one of the major murine Siglec receptors, in mHSP70-mediated effects. We asked whether mHSP70 could bind directly to Siglec-E. As a first approach, we generated a murine Siglec-E receptor construct encoding an HA tag in its N-terminal (extracellular) domain. We then transfected CHO-K1 cells with Siglec-E-HA plasmids and analyzed the binding and colocalization of the expressed receptor with fluorescently tagged mHSP70 in the absence of other potential receptors. Notably, wild-type (WT) CHO-K1 cells do not bind extracellular Hsp70 based on previous screening studies, providing a clean platform to examine the abilities of innate receptors to bind and respond to HSP70.^{9,10} Alexa 488-tagged mHSP70 bound to CHO-K1 expressing Siglec-E but not to the untransfected control cells (Figure 1(a)). Such binding was inhibited by an anti-Siglec-E antibody (Figure 1(a)). By confocal microscopy, we confirmed both that mHSP70 did not bind to CHO-K1 control cells (Supplementary Figure 1), and that it localized with HA (red, merged represented by yellow area) in Siglec-E-HA-expressing CHO-K1 cells (Figure 1(b)), with a Pearson's correlation of 0.098 ± 0.013 in CHO-K1 cells versus 0.792 ± 0.059 in CHO-Siglec-E-HA cells ($P < 0.0001$, Supplementary Table 1). To further confirm these findings, ELISA plates were coated with purified mHSP70 and probed with a recombinant soluble IgG-Fc fusion chimera containing the extracellular domain of Siglec-E (Figure 1(c)). mHSP70 interacted directly with Siglec-E under these conditions (Figure 1(d)), confirming the binding of the HSP70 to this receptor. We then examined HSP70 binding in primary DCs *ex vivo*. We incubated DCs isolated from naïve mice spleens with extracellular Alexa 488-tagged mHSP70 and evaluated their potential

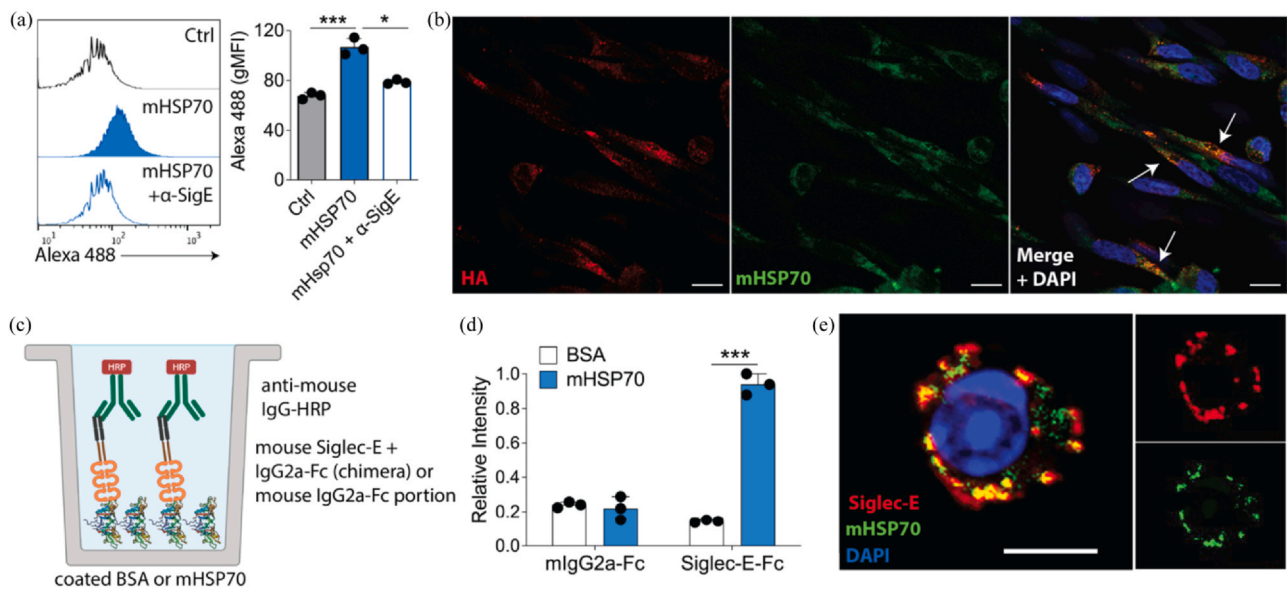


Fig. 1 mHSP70 binds to murine Siglec-E. (a) CHO-K1 cells stably overexpressing Siglec-E-HA were treated with Alexa 488-tagged murine HSP70 (mHSP70) on ice for 30 min, and its binding was evaluated by flow cytometry. Untransfected CHO-K1 cells treated with Alexa 488-mHSP70 were used as controls. Anti-Siglec-E blocking antibody was added to neutralize the binding. $*P < 0.05$ or $***P < 0.001$ when compared to mouse IgG using one-way analysis of variance with Tukey post-hoc test. (b) Representative confocal microscopy images of CHO cells stably overexpressing Siglec-E-HA and treated with Alexa 488-tagged mHSP70. Cells were then stained for HA (red). Magnification 400 \times . Scale bar = 5 μ m. (c) Representation of the ELISA in which plates were coated with mHSP70 or BSA (negative control), followed by incubation with a Siglec-E-Fc chimera and a secondary horseradish peroxidase anti-mouse IgG. Representation created with BioRender.com. (d) Relative binding between mHSP70 to Siglec-E-Fc determined by ELISA. $***P < 0.001$ when compared to BSA by t-test. (e) Representative confocal image of mHSP70 (green) binding to Siglec-E (red) in splenic DCs isolated from naïve wild-type mice with magnetic CD11c beads. Scale bar = 10 μ m. Bars are represented as mean \pm SD of triplicate. All data are representative of at least three independent experiments. Abbreviations used: mHsp70, mouse Hsp70; gMFI, geometric mean fluorescence intensity; BSA, bovine serum albumin.

colocalization with Siglec-E on the cells. mHSP70 colocalized with Siglec-E in the murine DCs as indicated by areas of the yellow merged fluorescence (Figure 1(e)), with a Pearson's correlation of 0.702 ± 0.127 . In conclusion, our data indicate that extracellular mHSP70 can bind to murine Siglec-E.

mHSP70 is a non-sialylated ligand for Siglec-E

Siglec-E was previously shown to bind specifically to glycosylated proteins.^{11,12} We thus asked whether the mHSP70 used in the study was glycosylated. However, our mHSP70 preparation did not contain detectable levels of N-glycans (Figure 2(a)), when compared with the heavily glycosylated fetuin, used as a positive control (Figure 2(b)). We confirmed these findings by SDS-PAGE and Western blot analyses. Deglycosylation of mHSP70 with the N-glycosidase PNGase F treatment did not result in a band shift in SDS-PAGE analysis, contrary to what was observed with fetuin (Figure 2(c)). Additionally, the potential presence of putative $\alpha(2,6)$ sialoglycans displayed on mHSP70 was further analyzed. Western blots showed that the lectin sambucus nigra lectin was not able to bind to mHSP70 (Figure

2(d)). These findings led us to hypothesize that Siglec-E recognizes an alternative peptide-based topology on the HSP molecule, unrelated to glycosylation.

Siglec-E and LOX-1 form innate receptor complexes in immune cells

Mammalian HSP70 has been previously demonstrated to bind to the innate receptor LOX-1.^{9,13} We next asked if Siglec-E and LOX-1 could interact and potentially form complexes in DCs, cooperating to fine-tune opposing signals, and consequently their inflammatory/anti-inflammatory effects. To test this hypothesis, we coated plates with purified LOX-1 and probed them with different concentrations of a soluble Siglec-E-Fc chimera (Figure 3(a)). An ELISA revealed that the binding occurred in a dose-dependent manner (Figure 3(b)) and was partially inhibited by an anti-LOX-1 antibody (Figure 3(c)). We then confirmed their interaction by immunoprecipitating Siglec-E from lysed murine splenocytes. Using immunoblot analysis, we detected considerable amounts of LOX-1 in the Siglec-E immunoprecipitate (Figure 3(d)). Interestingly, Siglec-E is also associated with endogenous mHSP70 present in the splenocytes (Figure 3(d)). We confirmed these findings by

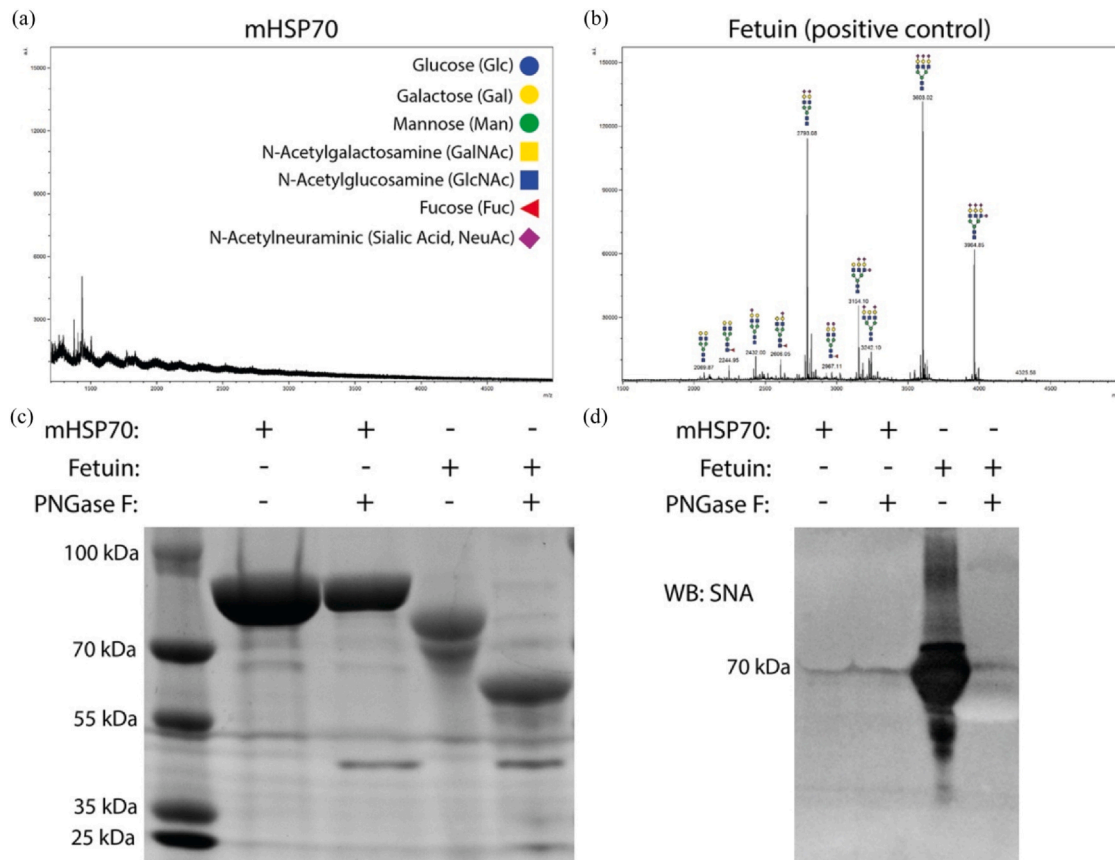


Fig. 2 Mouse Hsp70 is not glycosylated. (a) Analysis of N-glycans profile of extracellular mHsp70. (b) Fetuin was used as a positive control. MALDI-TOF mass spectrometry was performed in protein preparations in which the N-linked glycans were released enzymatically by PNGase F and permethylated, before being profiled. (c) SDS-PAGE of mHSP70 or fetuin treated or not with PNGase F (deglycosylation). (d) SNA lectin blot analysis of purified extracellular mHSP70 or fetuin (positive control) treated or not with PNGase F. (c) and (d) One representative gel from $n = 3$ biologically independent experiments. Abbreviation used: mHsp70, mouse Hsp70; MALDI-TOF, matrix-assisted laser desorption/ionization-time-to-flight; SNA, sambucus nigra lectin,

transfecting stable CHO-LOX-1-Myc cells with Siglec-E-HA plasmids and analyzing their interaction by confocal microscopy. Importantly, Myc and HA are expressed in the extracellular domain of LOX-1 and Siglec-E, respectively. When we transfected Siglec-E into CHO cells expressing LOX-1, we noticed that surface expression patterns changed dramatically when compared to WT CHO transfectants (Figure 3(e)). In nonpermeabilized CHO cells expressing only Siglec-E, receptor distribution seemed more evenly spread over the cell surface. However, Siglec-E expression became concentrated into foci in cells when cotransfected with LOX-1 (Figure 3(e)), suggesting an association in discrete patches on the membrane. By staining for HA and Myc tags, we observed that Siglec-E and LOX-1 colocalization could be detected in discrete foci in the CHO cells (arrows, Figure 3(f)). To further characterize Siglec-E/LOX-1 interaction in intact cells, we examined their colocalization in non-stimulated DCs isolated from murine spleens. Indeed, flow cytometry showed that $\sim 15\%$ of CD11c^{hi} cells coexpressed Siglec-E and LOX-1 on their cell surface, but

not in Siglec-E KO cells as expected (Figure 3(g) and (h)). Moreover, Siglec-E KO DCs express lower levels of LOX-1 than WT cells (Figure 3(i)). Overall, these results support a significant interaction between Siglec-E and LOX-1 on DCs.

Molecular docking and electrostatic potential analysis of the interaction between Siglec-E and LOX-1 extracellular domains

We next employed complementary bioinformatic analysis to further explore the molecular nature of the interactions between Siglec-E and LOX-1. We first generated *in silico* 3D models for both Siglec-E and LOX-1 receptors. The two best templates for Siglec-E were a myelin-associated glycoprotein from *Mus musculus* (PDB ID: 5LFR) and two N-terminal domains of SIGLEC-5 from *Homo sapiens* (PDB ID: 2ZG2). The whole extracellular moiety comprising residues 19 to 353 of Siglec-E was modeled using the multiple templates approach from *Modeller*. Regarding the murine LOX-1 protein (target), the best template structure

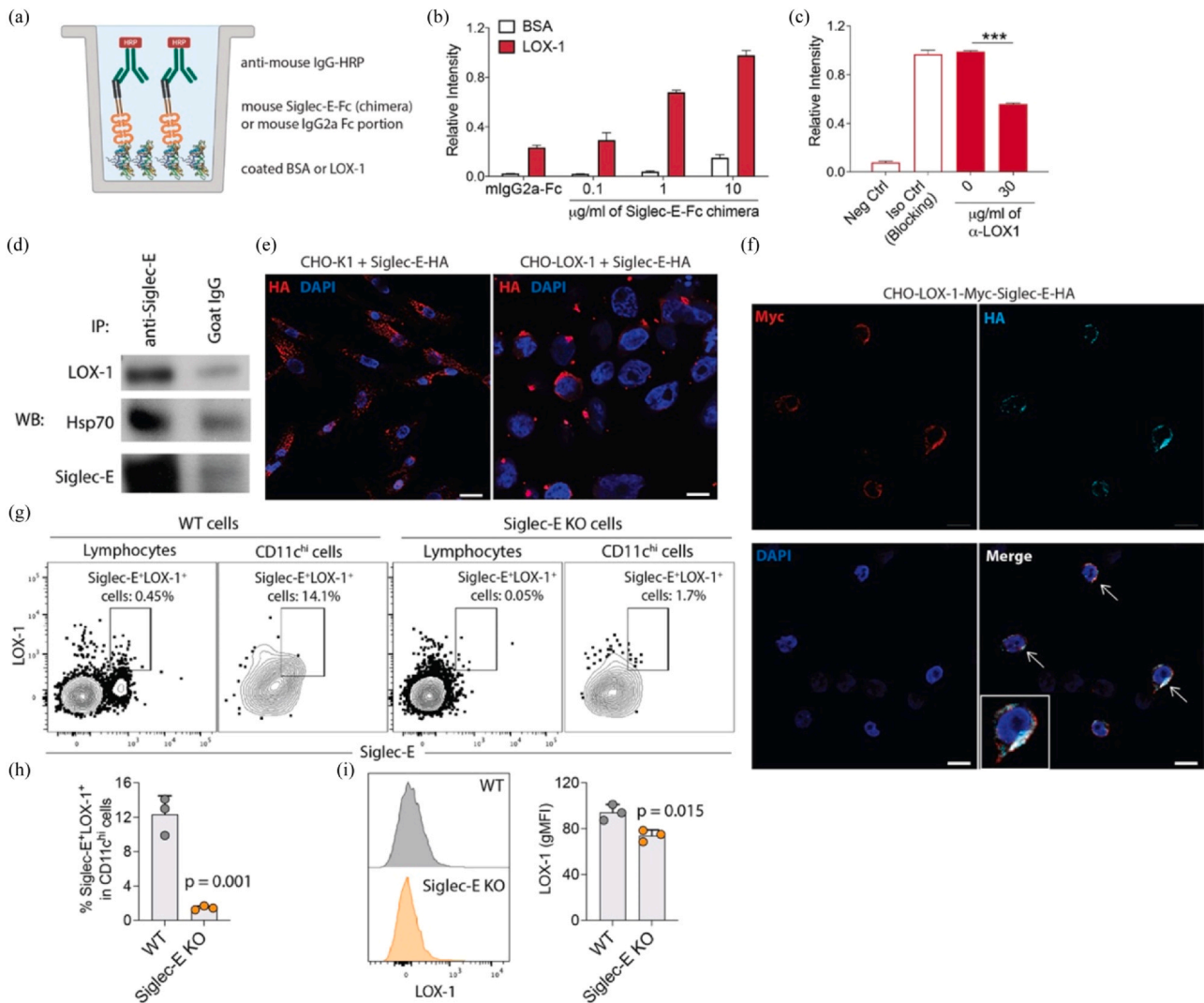


Fig. 3 Innate receptors Siglec-E and LOX-1 form hetero-complexes and are coexpressed by murine CD11c^{hi} DCs. (a) Cartoon of the ELISA in which LOX-1 or BSA (negative control) was coated in the plate, incubated initially with different concentrations of a soluble Siglec-E-Fc chimera, followed by incubation with a secondary HRP anti-mouse IgG. Representation created with BioRender.com. (b) Relative binding between LOX-1 and Siglec-E-Fc chimera is dose-dependent. The mIgG2a-Fc controls were used at 10 $\mu\text{g/ml}$. All assays were performed in triplicate. (c) Relative binding between LOX-1 and Siglec-E-Fc chimera in the presence of anti-LOX-1 blocking antibody or isotype control. *** $P < 0.001$ by one-way analysis of variance with Tukey post test. All assays were performed in triplicate. (d) Lysates from wild-type (WT) naïve spleen cells were precipitated with either Siglec-E-specific antibody or control mouse IgG. Precipitates were probed with antibodies to Siglec-E, LOX-1, or mHSP70. Complete membrane blots are included in [Supplementary Figure 1](#). One representative gel from $n = 3$ biologically independent experiments. (e) CHO-K1 cells or CHO cells stably overexpressing LOX-1 were transfected with a plasmid containing the Siglec-E-HA construct. Siglec-E expression pattern (HA staining, red) was analyzed by confocal microscopy in nonpermeabilized cells. (f) Representative confocal microscopy images of untreated CHO cells stably overexpressing LOX-1-Myc and Siglec-E-HA receptors stained for c-Myc (red) and HA (cyan) in nonpermeabilized cells. (e) and (f) Magnification 400 \times . Scale bar = 5 μm . All data are representative of three independent experiments. (g) Representative contour plots of Siglec-E⁺LOX-1⁺ cells in total lymphocytes or CD11c^{high} (DCs) cells from WT or Siglec-E KO naïve mice spleens. (h) Percentages of Siglec-E⁺LOX-1⁺ cells and (i) LOX-1 geometric mean fluorescence (gMFI) in CD11c^{high} cells from WT or Siglec-E KO naïve mice spleens. Representative plots from $n = 3$ biologically independent experiments with 3 animals per group. Statistical analyses by t-test.

found was the LOX-1 molecule from *Homo sapiens* (PDB ID: 1YPQ). Previous data indicate that mouse LOX-1 possesses the structural features required to form dimers, as it has been shown to occur with homologous human LOX-1.¹⁴ Also, the C-terminal C-type lectin-like

domain (CTLD) is highly conserved among species and was already shown to be involved in the binding of several molecules by C-type lectins such as LOX-1.^{15,16} For this reason, we decided to model the CTLD from LOX-1 as a homodimer and analyze *in silico* its

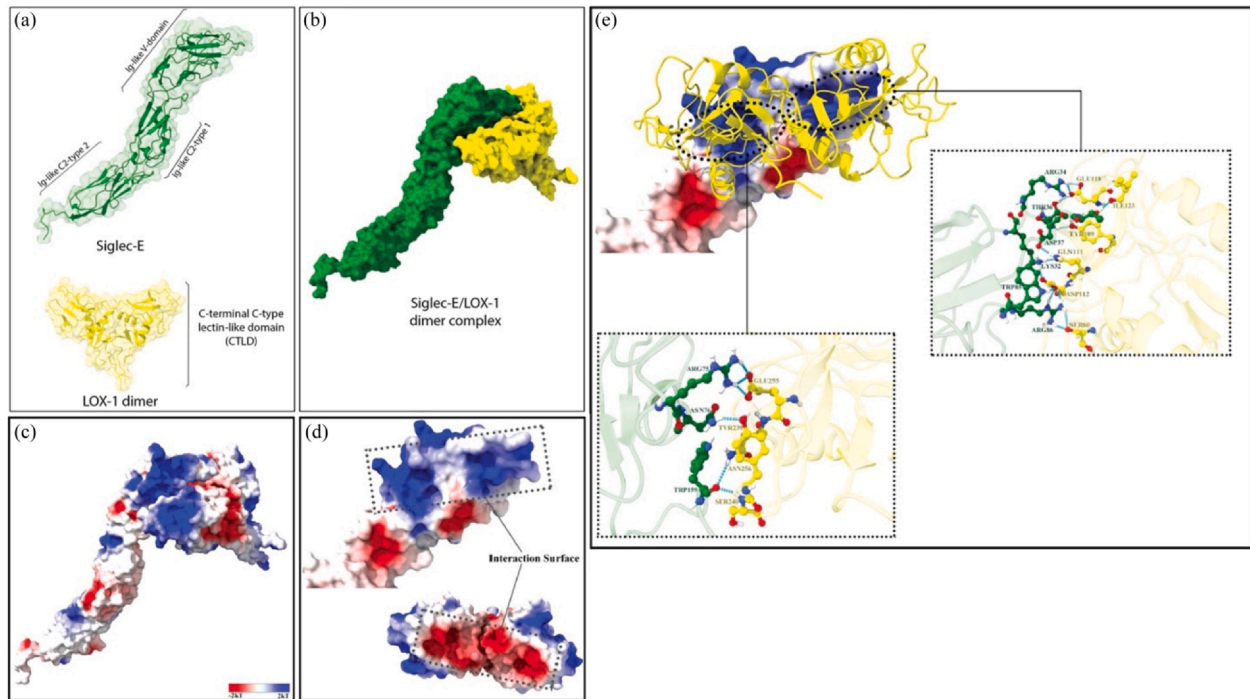


Fig. 4 *In silico* modeling of Siglec-E and LOX-1 dimer and molecular docking and electrostatic potential analysis of the Siglec-E/LOX-1 dimer complex. Models of Siglec-E (green) and LOX-1 dimer (yellow) domains are represented in (a). In (b), a representation of Siglec-E and LOX-1 predicted interaction was obtained from the ClusPro web server. (c) Complex with electrostatic potential computed on the surface, where red, white, and blue represent negative, neutral, and positive charges, respectively (gradient ranges from $-2kT$ to $2kT$, being k the Boltzmann constant and T the temperature). (d) The molecules were separated and rotated to show the interaction surface between Siglec-E and LOX-1, evidencing a complementarity of charges. (e) LOX-1 is positioned exactly over the two positive charges of Siglec-E, and the complex is stabilized by several hydrogen bonds (cyan blue) between Siglec-E (green) and LOX-1 (yellow).

interaction with Siglec-E. Data from *ClusPro*, a well-known molecular docking server used to predict protein-protein interaction,¹⁷ predicted that a portion of the Ig-like V-domain from Siglec-E could interact with the CTLD from LOX-1 dimers (Figure 4(a) and (b)). Of potential significance, there is a charge complementarity at the interaction surface between the extracellular domain of both molecules, where two positively charged motifs in Siglec-E interact with a negatively charged region of CTLD from LOX-1 (Figure 4(c) and (d)). We screened residues present at the Siglec-E/LOX-1 dimer interface, focusing on those involved in hydrogen bonding (Figure 4(e)). Most of the predicted interacting Siglec-E residues are positively charged, including ARG34, LYS32, ARG75, and ARG86, while the LOX-1 residues are negatively charged, ASP112, GLU118, GLU255, and ASN256 (Supplementary Table 2). We identified additional residues that could be involved in the interaction (Supplementary Table 2). Hydrogen bonding between the molecules appeared to involve ARG34, ARG75, and ARG86 from Siglec-E and GLU112, GLU118, GLU255, and SER60 from LOX-1. In conclusion, our modeling

studies suggest that potential electrostatic interactions could occur between Siglec-E and the LOX-1 within their extracellular domains, along with additional hydrogen bonds, which would be crucial to maintaining a heterodimer.

mHSP70 binds to Siglec-E/LOX-1 complexes present in lipid rafts

We next investigated whether mHSP70 could bind to the receptor complex formed by Siglec-E and LOX-1. To determine whether mHSP70 simultaneously binds to the receptor complex, we treated CHO-LOX-1-Myc-Siglec-E-HA cells with Alexa 488-tagged mHSP70. Fluorescently tagged mHSP70 colocalized with Siglec-E/LOX-1 complexes in CHO cells (Figure 5(a), Supplementary Table 3). We confirmed these findings by treating splenic primary DCs with fluorescently tagged mHSP70 at 4 °C to reduce endocytosis. mHSP70 bound to murine DCs and became colocalized with Siglec-E and LOX-1 (Figure 5(b)). Foci of colocalization (shown in white) were seen on the cell surface upon incubation with mHSP70, suggesting the presence of triple complexes between each mHsp70 (green), Siglec-

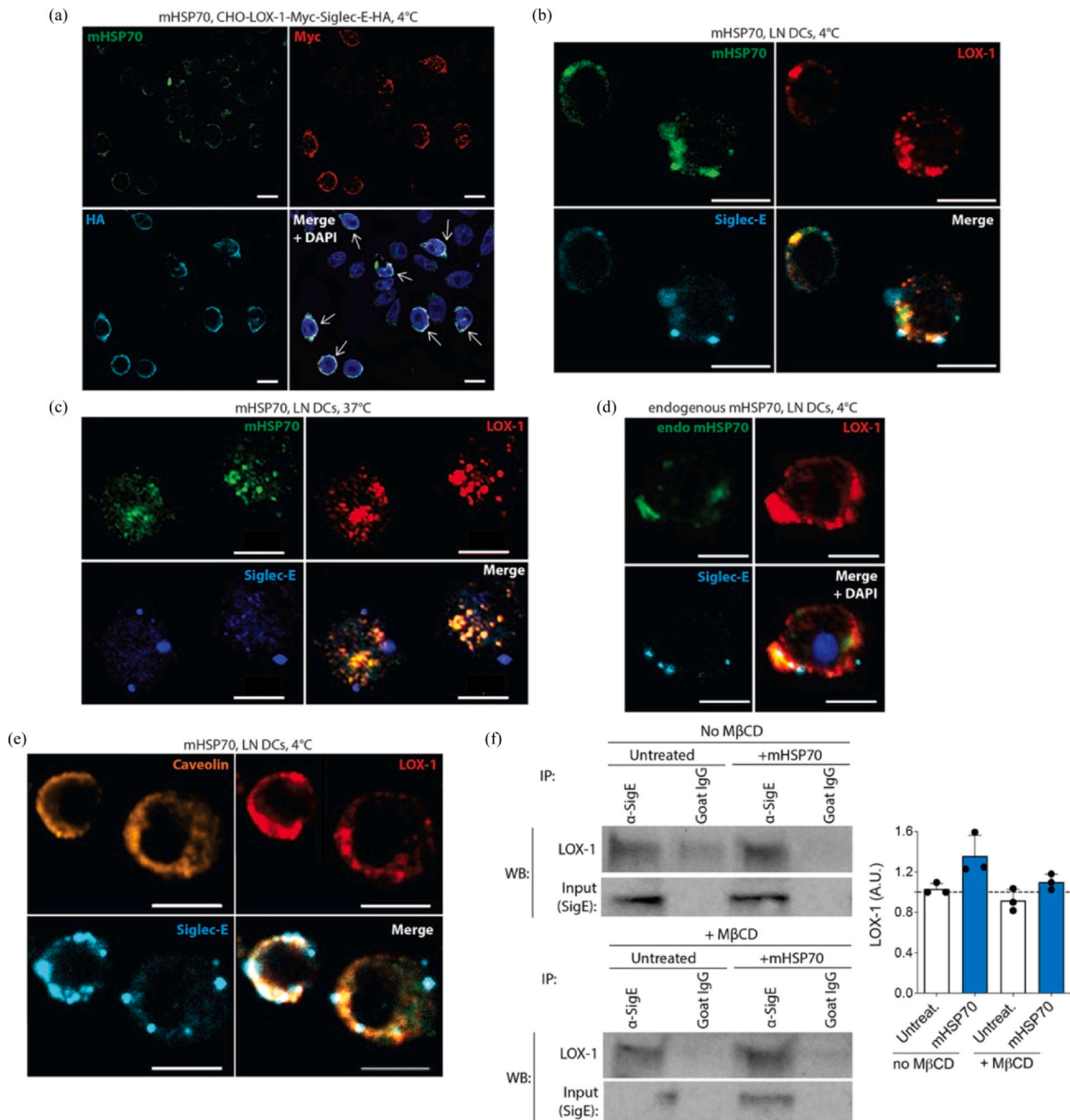


Fig. 5 Siglec-E/LOX-1 complexes are localized in lipid microdomains. (a) CHO-LOX-1-Myc-Siglec-E-HA expressing cells were treated with Alexa 488-tagged extracellular murine HSP70 (mHSP70, 10 μ g/mL) on ice for 30 min. Nonpermeabilized cells were then fixed and stained for c-Myc (red) and HA (Cyan) and analyzed by confocal microscopy. Representative confocal microscopy images of murine DCs isolated from naïve wild-type animals and treated with Alexa 488-tagged mHSP70 on ice (b) or at 37°C (c) for 30 min. Nonpermeabilized cells were then fixed and stained for LOX-1 (red) and Siglec-E (Cyan). (d) Representative confocal microscopy images of murine nonpermeabilized DCs stained for endogenous mHSP70 (green), LOX-1 (red), and Siglec-E (Cyan) at 4°C. (e) Representative confocal microscopy images of nonpermeabilized murine DCs stained for caveolin (orange), LOX-1 (red), and Siglec-E (Cyan) at 4°C (a–e). Magnification 400 \times . Scale bars = 5 μ m. (f) Wild-type splenocytes were treated for 2 h with methyl β cyclodextrin (20 mM, cholesterol-sequestering agent) before stimulation with mHSP70 for 30 min. Splenocyte lysates were precipitated with either Siglec-E-specific antibody or control goat IgG. Precipitates were probed with antibodies specific to LOX-1 or Siglec-E (input). One representative gel and densitometric analysis of the three biologically independent experiments. Complete membrane blots are included in [Supplementary Figure 1](#). Abbreviations used: DCs, dendritic cells; LOX-1, lectin-like oxidized low-density lipoprotein receptor-1; mHsp70, mouse Hsp70.

Table 1
Comparison of colocalization coefficients between Siglec-E and LOX-1 in untreated or mHSP70-treated murine dendritic cells.^a

Coefficients	Siglec-E-LOX-1 colocalization		
	Untreated	mHSP70	<i>P</i> value
Pearson's correlation	0.347 ± 0.078	0.543 ± 0.045	0.0157 ^b
Spearman's rank correlation value	0.383 ± 0.033	0.685 ± 0.041	0.0005 ^b

Abbreviations used: LOX-1, lectin-like oxidized low-density lipoprotein receptor-1; mHsp70, mouse Hsp70.

^aThe results are mean ± standard deviation of coefficients from five analyzed areas.

^bUntreated *versus* mHSP70, by t-test.

E (cyan), and LOX-1 (red) (Figure 5(b)). We also observed that mHSP70, Siglec-E, and LOX-1 complexes were internalized when conducting the binding assays at 37 °C (Figure 5(c)). These complexes are found at a physiological level since the stain of endogenous mHSP70 (green) colocalized with Siglec-E (cyan) and LOX-1 (red) on the membrane of murine DCs (Figure 5(d), Supplementary Table 4).

The focal concentrations of the Siglec-E/LOX-1 receptor complexes suggested that their association could occur in discrete patches on the membrane. Our previous studies on the Hsp70-binding scavenger receptors indicated that SRECI, a close functional homolog of LOX-1, was present in cholesterol-rich lipid rafts and could influence other immune signaling molecules to enter these lipid microdomains and regulate their activities.¹⁸ Therefore, we investigated the possibility that LOX-1 might possess a similar property compared to its scavenger receptor comember SREC-I. Indeed, Siglec-E (cyan) and LOX-1 (red) colocalized with the lipid raft marker Caveolin-1 (orange) in splenic mouse DCs (Figure 5(e), Pearson's correlation of 0.757 ± 0.143 and 0.911 ± 0.037, respectively). We further investigated whether Siglec-E and LOX-1 interaction would increase upon stimulus with mHSP70 by calculating different colocalization coefficients. Compared to untreated cells, DCs stimulated with mHSP70 presented significantly higher colocalization between Siglec-E and LOX-1, as demonstrated by a higher Pearson's correlation and Spearman's rank correlation values (Table 1).

To evaluate the potential role of lipid microdomains in stabilizing Siglec-E/LOX-1 complexes, we incubated WT splenocytes without or with cholesterol-sequestering agent methyl β cyclodextrin (MβCD), known to disrupt lipid microdomains. We then treated the cells with mHSP70 and immunoprecipitated Siglec-E from the lysates of the treated cells, probing for the presence of LOX-1 by immunoblot. A slight increase in LOX-1

coprecipitate was observed in lysates treated with mHSP70, an effect that was partially blocked in cells pre-treated with MβCD (Figure 5(f)). These data supported the conclusion that Siglec-E/LOX-1 complexes are concentrated within lipid microdomains.

Siglec-E controls the magnitude of the DC maturation triggered by LOX-1 ligands

We next asked whether Siglec-E was involved in regulating the responses triggered by LOX-1 ligands. We tested the activation status of murine WT or Siglec-E-deficient or bone-marrow-derived DCs (BMDCs) incubated with increasing doses of mHSP70 or oxidized LDL (oxLDL) (a classic LOX-1 ligand).¹⁹ To exclude confounding effects of other contaminating molecular patterns, we analyzed the effects of endotoxin-free preparations of BMDCs by measuring MHC II and CD86 using flow cytometry. Both oxLDL and mHSP70 increased the percentage of matured MHC II^{hi}CD86^{hi} DCs in a dose-dependent manner (Figure 6(a)). This elevation was notably more significant in the absence of Siglec-E (Figure 6(a)). Analysis of unstimulated Siglec-E KO BMDCs indicated elevated basal levels of MHC II^{hi}CD86^{hi} cells (Figure 6(a)), suggesting a different level of basal DC maturation state in these cells. This finding is consistent with the anti-inflammatory effects reported for Siglec-E.²⁰ Thus, the absence of Siglec-E potentiates the expression of maturation markers by BMDCs stimulated with LOX-1 ligands.

A prediction from these findings was that Siglec-E could potentially exert a negative regulatory effect on LOX-1-triggered intracellular signaling pathways. Given that LOX-1 signals through phosphorylated Src (p-Src) in DCs,²¹ we explored whether the impact on p-Src signaling is mediated by Siglec-E. In the absence of any ligand, Siglec-E KO BMDCs had increased baseline levels of p-Src compared to WT cells (Figure 6(b)). The treatment with either oxLDL or mHSP70 led to increased p-Src levels (Figure 6(b)). The upregulation of p-Src was notably more significant in Siglec-E-deficient DCs (Figure 6(b)). Siglec-E is also known to recruit SH2-domain-containing protein tyrosine phosphatases SHP-1 and SHP-2 through its tyrosine-based inhibitory motifs and tyrosine-based switch motif,²² thus dampening inflammatory responses.^{20,23} Hence, we examined the levels of one of the tyrosine phosphatases, SHP-1, upon oxLDL or mHSP70 treatments. As expected, Siglec-E KO BMDCs have lower baseline levels of SHP-1 (Figure 6(c)). Although oxLDL and mHSP70 increased SHP-1 levels in Siglec-E-deficient DCs, this effect was significantly reduced when compared to WT cells (Figure 6(c)).

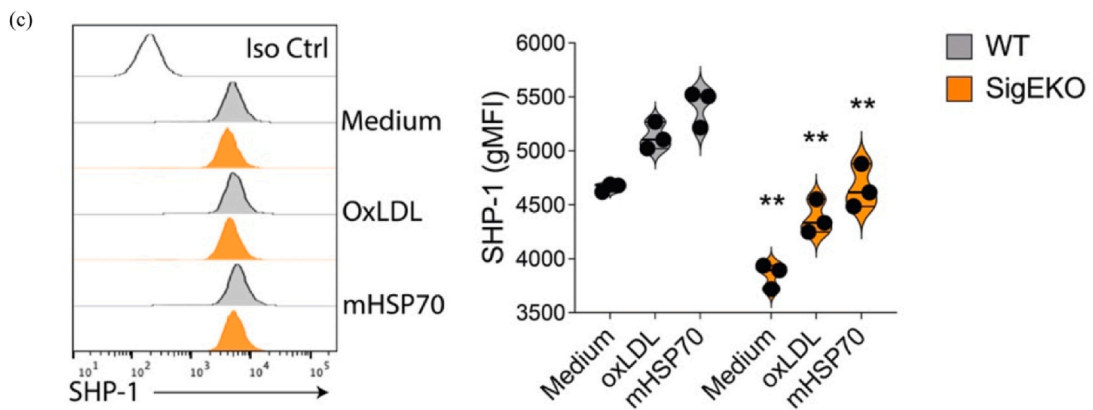
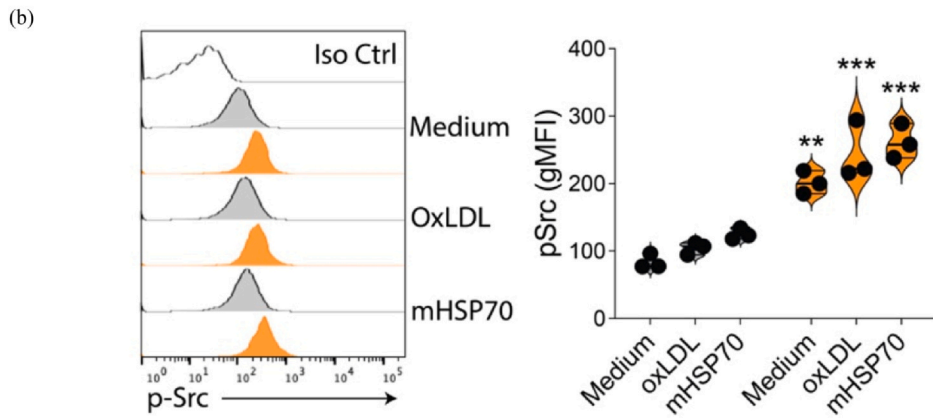
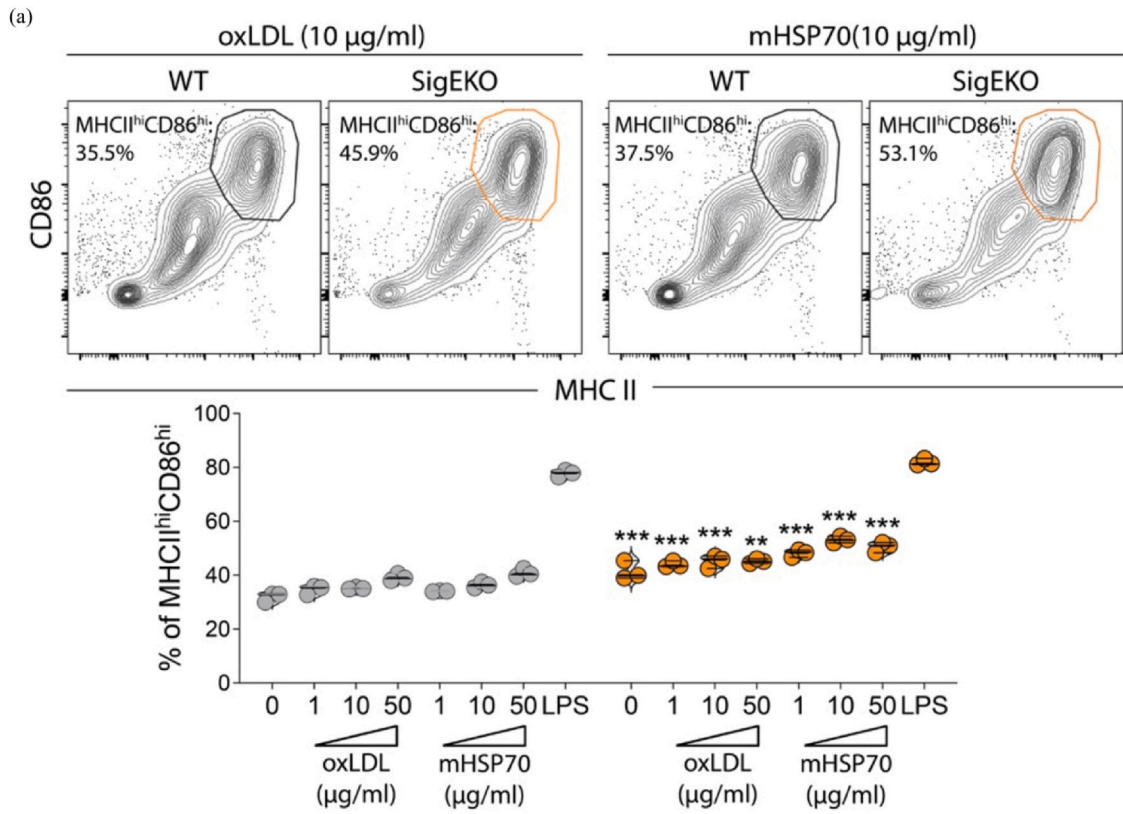


Fig. 6 The absence of Siglec-E increases LOX-1-mediated maturation of DCs. (a) Wild-type (WT) or Siglec-E KO (SigEKO) bone-marrow-derived dendritic cells were treated with increasing doses of oxLDL or mHSP70 for 24 h, and MHC II^{hi}CD86^{hi} cells were evaluated by flow cytometry. ***P* < 0.01, ****P* < 0.001 compared to WT by one-way analysis of variance (ANOVA) with Tukey post test. The experiments represent two repetitions performed in triplicate of a pool of two mice per genotype. **P* < 0.05, ***P* < 0.01, ****P* < 0.001 compared to WT by one-way ANOVA with Tukey post test. WT cells are represented in gray, and Siglec-E KO in orange. WT or Siglec-E KO bone-marrow-derived dendritic cells were treated with 50 µg/mL of oxLDL or 50 µg/mL of mHSP70 for 30 min, and the expression of (b) phospho-Src (p-Src) or (c) SHP-1 was assessed using flow cytometry. ***P* < 0.01, ****P* < 0.001 when compared to WT by one-way ANOVA with Tukey post test. Abbreviations used: Iso Ctrl, isotype control; LOX-1, lectin-like oxidized low-density lipoprotein receptor-1; mHsp70, mouse Hsp70; oxLDL, oxidized LDL.

Discussion

Our study describes a novel innate receptor complex formed by LOX-1 and Siglec-E that mediates responses to extracellular Hsp70. Innate immune responses to cell damage can induce inflammation and even adaptive immunity.^{24,25} However, the magnitude of each of these inflammatory responses is highly regulated in realistic scenarios; inflammation in response to cell damage is generally thought to lead to tissue repair rather than high-affinity antibodies or cytotoxic T memory, minimizing potential risks for autoimmunity. Tissue damage is thought to be perceived differently in the absence or presence of infection. Significant evidence supports the idea of different receptors engaged by ligands that we classify as pathogen-associated molecular patterns *versus* the ones we call damage-associated molecular patterns.²⁶ This model, however, still does not indicate if receptors that evolved to recognize molecular patterns associated with cell damage can distinguish these structures from conserved microbial orthologs.

The binding of the scavenger receptor LOX-1 by human and mHsp70^{9,13,27} was previously shown to induce TNF- α and deliver antigens to APCs, resulting in the enhancement of anti-tumor immunity and tumor regression in the absence of significant autoimmunity.^{28–30} This was rather puzzling because no regulatory mechanism had been invoked or shown that would prevent possible pathological autoimmune responses. Recently, Fong *et al.*⁸ demonstrated that human HSP70 can bind to the human-paired receptors Siglec-5 and Siglec-14. Their findings suggested a possible mechanism for fine-tuning this inflammatory response: while Siglec-14 enhanced the production of IL-8 and TNF- α in human monocytes after stimulation with human HSP70, expression of Siglec-5 reduced this inflammatory signaling. Some members of the Siglec family receptors function *via cis* interactions,^{31,32} by sequestering ligands away from their receptors and by trans-interacting with their ligands, thus regulating immune responses to self.³³ Our results suggest that Siglec-E, an important Siglec receptor expressed in mouse innate immune cells, regulates the downstream responses of LOX-1 when it engages mHSP70 or oxLDL.

We propose that Siglec-E can control the threshold for DC activation, contributing to distinguishing signal from noise triggered by self-molecules.³⁴

The responses to mHSP70 are complex and depend largely on context. The source of mHSP70 may result in distinct post-translational modifications,⁷ while its subcellular location can also influence the downstream immune response. For instance, Hsp70 is released into the extracellular space, likely *via* plasma membrane-associated vesicles, which show an enhanced ability to activate macrophages, as indicated by elevated TNF- α production.^{35,36} An evolutionary model for plasma membrane-associated Hsp70 was first proposed by De Maio and Hightower.³⁷ Moreover, binding of mHSP70 to LOX-1 does not always result in T cell responses but rather consistently shows induction of TNF- α ^{2,4}, and might even result in IL-10 production.³⁸ This range of responses might reflect a differential expression of the Siglec-E/LOX-1 receptor complex in the relevant APCs in each experimental system. For example, TNF- α and IL-10 induction might reflect binding to LOX-1 complexed to Siglec-E, leading to inflammation and subsequent tissue repair, while binding to LOX-1 in the absence of Siglec-E association might favor the anti-tumor immunity outcomes previously reported. In light of this hypothesis, Siglec-E was recently demonstrated to interact with the scavenger receptor CD36 and control the development of atherosclerosis in mice.³⁹

Finally, we have found the localization of the receptors within discrete lipid microdomains to be important for the signaling pathways triggered by the Siglec-E/LOX-1 complex. Lipid rafts are known to stabilize extensive cell surface signaling complexes, leading to the formation of immunological synapses.^{40,41} These data suggest that cell surface interaction between LOX-1 and Siglec-E may be required to stabilize both receptors in functional forms and could potentially lead to larger complexes at the cell membrane, as observed when LOX-1 binds to ox-LDL.⁴² Our data suggest that large signaling complexes, which include LOX-1, Siglec-E, and other possible receptors or associated proteins, are formed during immunological responses to extracellular HSPs and perhaps other agents. Future studies should assess whether human LOX-1 has a Siglec-binding

partner, such as Siglec-7 and Siglec-9, which are close human paralogs to murine Siglec-E.⁴³ It was recently suggested that Siglec-E can assume a disulfide-linked dimer configuration.⁴⁴ The homodimeric interaction is formed through a disulfide bond between cysteines at position 298, which is on the opposite side of the predicted Siglec-E/LOX-1 interface. Thus, although the interaction between Siglec-E and LOX-1 is likely between two dimers on the cell surface, the Siglec-E/LOX-1 interface would not be affected by the presence of a second Siglec-E molecule. Also, Siglec-E is itself N-glycosylated and likely carries sialic acid residues.⁴⁴ This modification could be important for determining the interaction with LOX-1. However, the potential role of sialic acid interactions in this process has yet to be determined. Based on other examples, this modification could range from being critical¹¹ to practically unimportant.^{45,46} The composition of innate immune receptors within these complexes could explain whether a response would be biased towards inflammatory or anti-inflammatory outcomes, as well as its duration and amplitude. It also seems from our data that DCs or macrophages might include both free receptors as well as Siglec-E/LOX-1 complexes.⁴⁷ Free receptors may be in transit to forming the hetero-complexes and may require ligand association to progress through membranes to form the complexes, or individual receptors might have discrete stand-alone functions.

Conclusion

Our study highlights the critical role of the LOX-1/Siglec-E receptor complex in modulating immune responses to extracellular Hsp70. This interaction provides a potential regulatory mechanism that balances inflammation and immune activation. The presence of Siglec-E appears to fine-tune the immune response, potentially directing outcomes toward tissue repair or immune activation, depending on the context. Additionally, the localization of these receptors within lipid microdomains suggests an essential structural component in stabilizing signaling pathways, suggesting that cellular context and receptor configuration significantly influence immune outcomes. The differential expression of this receptor complex likely explains the variable responses to Hsp70 observed across experimental systems, from pro-inflammatory TNF- α production to anti-inflammatory IL-10 release. Future research should investigate analogous receptor partnerships in humans, particularly examining whether human LOX-1 interacts with Siglec-7 or Siglec-9, and further explore how the composition and organization

of these receptor complexes determine the nature, magnitude, and duration of innate immune responses to cellular damage.

Materials and methods

Cell culture

WT CHO-K1 cells and all stable CHO transfectant cells were grown in Ham's F-12 medium (Gibco) supplemented with 10% FBS (Gibco). In the case of stable transfectant CHO-LOX-1 clonal selection was kept at 0.4 mg/mL G418 (Gibco). Stable CHO-Siglec-E transfectant was produced through transfection with pcDNA3.1+/N-HA mouse Siglec-E plasmid. Populations of G418 (0.4 mg/mL)-resistant cells were generated after 2 weeks of cell culture. In some experiments, CHO-LOX-1 cells were transiently transfected with a Siglec-E encoding construct. All cells were maintained in a 5% CO₂ humidified incubator.

Animals

C57BL/6 WT mice were obtained from The Jackson Laboratory (Bar Harbor, ME). C57BL/6 Siglec-E KO mice described previously in McMillan *et al.*⁴⁸ were not used because of concerns about the effect of the genomic Neo insertion. Instead, we used recently derived floxed exon-deleted Siglec-E KO mice.⁴⁹ Both males and females were used in the experiments. All animals were between 6 and 11 weeks old.

Experiments were approved by the BIDMC Animal Care and Use Committee under IACUC0792012 and Massachusetts General Brigham Institutional Animal Care and Use Committee 2016N000250 and 2020N000125. All animals were housed in accordance with the Institutional Animal Care and Use Committee and National Institutes of Health Animal Care guidelines.

Purified murine HSP70 and fluorescence labeling

ADP-bound mHsp70 was purified from mice liver, as previously described by Murshid *et al.*⁵⁰ Purified proteins were labeled with Alexa Fluor 488 fluorescent dye using Microscale Protein Labeling Kits from Thermo Fisher, following the manufacturer's instructions. Endotoxin levels were measured using the ToxinSensor Chromogenic LAL Endotoxin Assay Kit (Genscript), according to the manufacturer's instructions. Only proteins from 0.2 to 0.45 EU/mL were used in this

study. All proteins were quantified with the Pierce BCA Protein assay kit (Thermo Scientific) before use.

Siglec-E:Ligand ELISA interaction assay

The ELISA assay was performed as an adapted protocol from Fong *et al.*⁸ and Horie *et al.*⁵¹ Briefly, wells of a 96-well plate were coated overnight at 4 °C with 10 µg/mL of purified proteins in carbohydrate buffer (15 mM Na₂CO₃ and 35 mM NaHCO₃, pH 9.6), 100 µL per well. The wells were washed three times with PBS containing 0.1% Tween-20 (PBS-T) after each step. After blocking with 200 µL of blocking buffer (20 mM Tris HCl [pH7.4], 150 mM NaCl, and 1% BSA) for 1 h at room temperature (RT), 5 µg/mL of recombinant mouse Siglec-E-Fc chimera (R&D Systems, Cat. 5806) in 100 µL of buffer (10 mM Tris-HCl [pH7.4], 150 mM NaCl, 10 mM CaCl₂, 1% BSA and 0.05% Tween-20) was added to each well for 2 h at RT. For some experiments, 30 µg/mL of anti-LOX-1 blocking antibody (polyclonal, R&D Systems) or goat IgG isotype (Biolegend) control was added to the plate for 2 h at RT before adding the recombinant Siglec-E-Fc chimera. Next, the wells were incubated with horseradish peroxidase (HRP)-conjugated goat anti-mouse IgG (polyclonal, Abcam-ab6789, 1:3000) for 1 h, RT. HRP development was assayed by incubation with 3,3',5,5'-tetramethylbenzidine liquid substrate at RT for 30 min, and the reaction was stopped by adding 0.5 N HCl per well (both from R&D Systems). All IgG controls were used at equimolar concentrations for the highest experimental condition. Samples were analyzed at 450 nm using the Benchmark Plus microplate spectrophotometer (Bio-Rad).

DCs generation and isolation

DCs were grown from WT or Siglec-E KO bone marrows (BMDCs) in the presence of 40 ng/mL of granulocyte-macrophage colony-stimulating factor and IL-4 (both from Peprotech or Biolegend). Cells were cultured in 24-well plates in DMEM (Gibco), 10% FBS (Gibco) with pen/strep (Gibco). Non-adherent cells (DCs) were separated from adherent cells after six days in culture and were plated with 10 ng/mL of granulocyte-macrophage colony-stimulating factor and IL-4. On the next day, BMDCs were incubated in media (control), or different concentrations of mHSP70 or oxLDL (Thermo Fisher) for different time points. Cells were analyzed by flow cytometry.

CD11c⁺ cells were isolated from WT or Siglec-E KO naïve mice. Spleens were disrupted against a nylon screen and treated with Collagenase D (Roche) for 30 min at 37 °C. Cells were labeled with anti-CD11c

(clone N418)-coated magnetic beads (Miltenyi). Splenocytes were Fc-blocked, and CD11c⁺ cells were purified by positive selection using MACS separation columns (Miltenyi). The purity of selected cells was controlled by flow cytometry analysis. Purified DCs were analyzed by confocal microscopy.

Binding assays

BMDCs or splenic isolated DCs were grown on Poly-D-Lysine-coated coverslips (Corning) for 48 h in serum-free AIM-V media (Gibco). Cells were incubated on ice with 10 µg/mL of Alexa 488-labeled mHSP70 or DnaK for 20 min. For receptor-mediated internalization experiments, cells were incubated with labeled mHSP70 on ice for 20 min and then at 37 °C for 20 min. Coverslips were washed with PBS and fixed with 4% paraformaldehyde for immunofluorescence experiments as described below.

Bindings analysis by flow cytometry was performed as described.⁹ Briefly, nontrypsinized CHO cells were washed twice in PBS containing 0.5% FBS, 0.05% NaN₃, and 1 mM CaCl₂ (PFNC). For Siglec-E blocking, cells were incubated with 10 µg/mL of anti-Siglec-E antibody for 20 min at RT. Cells were washed twice and incubated with 10 µg/mL of labeled mHSP70 for 30 min on ice with gentle shaking. The cells were washed four times in PFNC twice, and the cells were analyzed in a FACS Canto II (BD Biosciences) flow cytometer.

Immunofluorescence

After fixing with 4% paraformaldehyde, cells were permeabilized (for visualizing intracellular proteins) or not (for surface expression or binding) using 0.1% Triton X-100. Samples were blocked with 3% normal goat serum (Sigma) for 1 h at RT. Cells were then stained with primary antibodies for 1 h at room temperature, and washed three times with 1× PBS. After that, cells were stained again with fluorophore-conjugated secondary antibodies for 1 h at room temperature. After three washes with 1× PBS, cells were stained with 1 µg/mL of Hoechst 33342 (Thermo Scientific) in PBS for 10 min at RT. Fluorophores were visualized using the following filter sets: 488 nm excitation and bandpass 505–530 nm emission filter for Alexa 488; 543 nm excitation and bandpass 560–615 nm for Cy3/Alexa 594 nm; and 633 nm excitation, in a Zeiss Confocal Microscope. Images were processed using ZEN 2 blue edition and Adobe Photoshop. Primary antibodies used were: goat anti-mouse Siglec-E (polyclonal IgG, R&D Systems) and mouse anti-cell membrane Hsp70 (clone 1H11, StressMarq) were used as 1:100, rat anti-LOX-1

(polyclonal, from Dr Sawamura, described in⁵² was used at 1:200, mouse anti-HA antibody (clone 16B12, Covance) at 1:250, rabbit anti-caveolin (polyclonal, Sigma-Aldrich) and mouse anti-c-Myc (clone 9E10, Biologend) were used as 1:300; rabbit anti-HA (cat H6908, Sigma) was used at 20 µg/mL. All secondary antibodies were purchased from Jackson ImmunoResearch and used as 1:300. All antibodies were prepared in 3% normal goat serum solution.

Deglycosylation of mHSP70

mHSP70 or fetuin (New England Biolabs, positive control) were subjected to cleavage by PNGase F (New England Biolabs), following the manufacturer's instructions. Briefly, for each reaction, 20 µg of mHSP70 and fetuin were denatured at 100 °C for 10 min and then mixed with Glycobuffer, 10% NP-40, and 1 µL of PNGase F, during 1 h at 37 °C. For protein detection, the gel was stained using Coomassie Blue (Bio-Rad).

Immunoprecipitation

WT splenocytes were incubated with 10 µg/mL of mHSP70 or media for 30 min at 37 °C. For some experiments, spleen cells were pre-treated with 20 mM of the cholesterol-sequestering agent M β CD (Sigma) for 4 h. After that, Siglec-E was immunoprecipitated. Spleen cells lysates were prepared in NP-40 lysis buffer (containing 1% Nonidet P-40, 150 mM NaCl, 1 mM EDTA, 1 mM PMSF-Boston BioProducts) with 1 \times Halt protease inhibitor cocktail (Thermo Scientific). Samples were pre-cleared with 40 µL of protein G Sepharose beads (50% slurry, GE Healthcare) plus 5 µg Goat IgG (Invitrogen), overnight at 4 °C with rotation. Protein concentration was measured with BCA assay and 350 µg of lysates were incubated with 5 µg of anti-Siglec-E antibody (polyclonal goat IgG-R&D Systems-cat. AF5806) or goat IgG for 2 h at 4 °C, and then 40 µL of 50% bead slurry was added for overnight at 4 °C with rotation. The beads were washed four times with lysis buffer, and complexes were eluted by boiling in Laemmli sample buffer (Bio-Rad) for western blot.

Western blot

For Western blotting, 30 µg of protein were resolved by 4–15% gradient SDS-PAGE (Bio-Rad) and transferred to polyvinylidene difluoride membranes. Membranes were blocked with 5% non-fat milk and immunoblotted with primary antibodies. After washing, membranes were incubated with secondary antibodies that are HRP-conjugated. The membrane reactions were visualized by

Perkin Elmer enhanced chemiluminescence reagents. Primary antibodies: goat anti-mouse Siglec-E (polyclonal IgG, R&D Systems) and mouse IgM anti-mouse Siglec-E (clone F-7, Santa Cruz) were used as 1:200, rabbit anti-LOX-1 (clone EPR4025, Abcam), and mouse anti-HSP70 (clone C92F3A-5, StressMarq) were used as 1:10,000. Secondary HRP-conjugated antibodies: goat anti-mouse IgM (Santa Cruz, cat. Sc-2064) was used as 1:2000, horse anti-mouse IgG (cat. 7076, Cell Signaling) was used as 1:3000, mouse anti-rabbit IgG, light chain-specific (clone 5A6-1D10, Jackson ImmunoResearch), and goat anti-rabbit IgG (cat. 7074, Cell Signaling) was used as 1:3000.

For western blotting with the lectin, the membranes underwent a 30-minute blocking at RT using 1 \times carbo-free blocking solution (Vector) containing 1% Tween-20 (Sigma). The membranes were then blotted with 1 µg/mL biotinylated Sambucus nigra Lectin (sambucus nigra lectin, EBL, Vector) in the TBS with 0.1 M Ca²⁺ and 0.1 M Mg²⁺ for 1 h at RT. Following three washes with PBS 1 \times with 0.05% Tween-20, membranes were incubated with goat anti-biotin-HRP at 1:5000 (Vector) in PBS 1 \times . Sialylated proteins on the membranes were visualized by PierceTM ECL Western Blotting substrate solution (ThermoFisher).

Flow cytometry

Cells were initially washed with PBS and stained with Fixable Viability Dye eFluor 780 (eBioscience) to detect dead cells. Cells were then Fc blocked for 20 min on ice, and surface markers were stained by incubation for 30 min with antibodies in PBS with 2% fetal bovine serum (FBS). Intracellular staining was performed after treating cells with the eBioscience[®] Foxp3 Fixation/Permeabilization solution, followed by incubation with antibodies for 1 h at RT. The following antibodies were used for murine cells: I-A^b (MHC II, clone AF6-120.1; 1:200), CD86 (clone GL1; 1:100), CD11c (clone HL3; 1:100), CD45R/B220 (clone RA3-6B2; 1:200), CD11b (clone M1/70; 1:100) from BD Biosciences; LOX-1 (clone 214012, 1:50) from R&D Systems; Siglec-E (clone M1304A01, 1:200) from Biologend.

For intracellular signaling pathway analysis, cells were fixed with 4% paraformaldehyde for 10 min at room temperature, followed by permeabilization with the True-Phos Perm buffer (Biologend) for 20 min on ice, followed by incubation with antibodies for 30 min at RT. The following antibodies were used for the signaling pathways: phospho-Src (Tyr418, clone SC1T2M3; 1:10) from Thermo Fisher, mouse IgG2b isotype control from Biologend, SHP-1 (clone E1U6R, 1:50), and rabbit IgG isotype control from Cell Signaling. Cells were

analyzed using FACS Canto II or Fortessa X-20 (both from BD Biosciences). Data obtained were analyzed using FlowJo software (version X, Tree Star).

Protein homology modeling and molecular docking

The proteins LOX-1 (Uniprot ID: Q9EQ09) and Siglec-E (Uniprot ID: Q91Y57) were modeled using Modeller v9.10 software.⁵³ Both proteins were initially submitted to the same homology modeling protocol. Briefly, we first searched for three-dimensional templates using BLAST, HHPRED, and PHYRE2 servers.^{54,55} Then we performed a structural alignment using selected templates against LOX-1 or Siglec-E sequences through the TCOFFEE server⁵⁶ to choose the best template(s). After that, a basic Modeller algorithm generated 100 models. The best model was chosen according to DOPE score, Ramachandran plot analysis, QMEAN score,⁵⁷ and ModFOLD6 score^{58,59} of each residue. A loop refinement was used to correct loop regions with bad modeling scores when necessary. The protein-protein interaction was assessed through ClusPro 2.0.¹⁷ The parameters were maintained as default. The electrostatic potential of the structures was computed with DelPhi software (available at <http://honig.c2b2.columbia.edu/>) and analyzed with UCSF Chimera and UCSF Chimera X software.^{60,61}

Statistics

For the comparison of two independent groups, we used an unpaired Student's t-test. For the multiple-group comparison, one-way or two-way analysis of variance (ANOVA) was used to determine differences. We used Tukey post-hoc tests for multiple comparisons between levels for one-way ANOVA and Sidak's multiple comparisons test for two-way ANOVA. Significant differences were set for $P \leq 0.05$. After Kaplan–Meier survival curves were generated, a log-rank test was used for statistical inference between experimental groups. Prism software was used for statistical analysis and plotting graphs (GraphPad Software, Inc.).

Funding and support This work was supported by Fundação de Amparo à Pesquisa do Estado do Rio Grande do Sul Grant 11/0903-1 and Financiadora de Estudos e Projetos Grant 01.08.0600-00 to CB, National Institutes of Health (NIH) grant number R01AI143887 to LVR, NIH grant number R01GM32373 to AV, NIH grant number R01CA119045 to SKC. LVR received support from the Department of Defense (RT190059, Award No. W81XWH-20-1-0758). Opinions, interpretations, conclusions, and recommendations are those of the author and are not necessarily endorsed by the Department of Defense. TJB was a recipient of an American Heart Association Postdoctoral

Fellowship (20POST35210659) and is currently a recipient of an American Heart Association Career Development Award (23CDA1049388). CB is a recipient of a 1B Productivity Fellowship from CNPq.

CRedit authorship contribution statement **Thais J. Teani:** Investigation, Formal analysis. **Benjamin J. Lang:** Writing – review & editing, Investigation, Formal analysis. **Maurício M. Rigo:** Writing – review & editing, Visualization, Investigation, Formal analysis. **Isadora T. Lape:** Writing – review & editing, Visualization, Project administration, Investigation. **Ayesha Murshid:** Writing – review & editing, Visualization, Methodology, Investigation, Formal analysis. **Karina Lima:** Writing – review & editing, Visualization, Investigation, Formal analysis. **Thiago J. Borges:** Writing – review & editing, Writing – original draft, Visualization, Investigation, Funding acquisition, Formal analysis, Conceptualization. **Stuart K. Calderwood:** Writing – review & editing, Writing – original draft, Supervision, Funding acquisition, Conceptualization. **Cristina Bonorino:** Writing – review & editing, Writing – original draft, Supervision, Funding acquisition, Conceptualization. **Leonardo V. Riella:** Writing – review & editing, Writing – original draft, Supervision, Funding acquisition. **Shoib S. Siddiqui:** Writing – review & editing, Investigation.

Author contributions T.J.B., A.M., M.M.R., L.V.R., C.B., and S.K.C. designed the research. T.J.B., K.L., and A.M. performed binding assays. T.J.B. and A.M. performed immunofluorescence. T.J.B., T.J.T., and S.S.S. performed ELISA assays. A.M. T.J.B., K.L., and I.T.L. performed dendritic cell cultures. T.J.B. and K.L. performed flow cytometry and Luminex experiments. T.J.B., A.M., and B.J.L. created CHO cell lines. I.T.L. maintained all the cell lines. M.M.R. performed in silico docking analyses. T.J.B., L.V.R., C.B., and S.K.C. wrote the manuscript. All authors edited the manuscript.

Data availability statement Data will be made available on request.

Declarations of interest The authors declare that they have no known competing financial interests or personal relationships that could have appeared to influence the work reported in this paper.

Acknowledgments We want to thank Dr Ajit Varki from the UC San Diego for useful materials and critical discussions, Dr Jawahar Mehta from the University of Arkansas for Medical Sciences for provided mice, Dr Tatsuya Sawamura from the Shinshu University for provided antibody, Lay-Hong Ang from the BIDMC Confocal Imaging Core for the assistance in immunofluorescence experiments, and Sylvain Lehoux from the BIDMC Glycomics Core for the assistance in glycosylation experiments.

Appendix A. Supplementary data

Supplementary data associated with this article can be found online at [doi:10.1016/j.cstres.2025.100083](https://doi.org/10.1016/j.cstres.2025.100083).

References

1. Iwasaki A, Medzhitov R. Control of adaptive immunity by the innate immune system. *Nat Immunol.* 2015;16:343–353.

2. Calderwood SK, Gong J, Murshid A. Extracellular HSPs: the complicated roles of extracellular HSPs in immunity. *Front Immunol.* 2016;7:159.
3. Borges TJ, Murakami N, Machado FD, et al. March1-dependent modulation of donor MHC II on CD103+ dendritic cells mitigates alloimmunity. *Nat Commun.* 2018;9:3482.
4. Borges TJ, Wieten L, Van Herwijnen MJC, et al. The anti-inflammatory mechanisms of Hsp70. *Front Immunol.* 2012;3:1–12.
5. Borges TJ, Lopes RL, Pinho NG, Machado FD, Souza APD, Bonorino C. Extracellular Hsp70 inhibits pro-inflammatory cytokine production by IL-10 driven down-regulation of C/EBP β and C/EBP δ . *Int J Hyperthermia.* 2013;29:455–463.
6. Borges TJ, Porto BN, Teixeira CA, et al. Prolonged survival of allografts induced by mycobacterial Hsp70 is dependent on CD4+CD25+ regulatory T cells. *PLoS One.* 2010;5:e14264.
7. Rigo MM, Borges TJ, Lang BJ, et al. Host expression system modulates recombinant Hsp70 activity through post-translational modifications. *FEBS J.* 2020 [https://doi: 10.1111/febs.15279](https://doi.org/10.1111/febs.15279).
8. Fong JJ, Sreedhara K, Deng L, et al. Immunomodulatory activity of extracellular Hsp70 mediated via paired receptors Siglec-5 and Siglec-14. *EMBO J.* 2015;34:2775–2788.
9. Thériault JR, Mambula SS, Sawamura T, Stevenson MA, Calderwood SK. Extracellular HSP70 binding to surface receptors present on antigen presenting cells and endothelial/epithelial cells. *FEBS Lett.* 2005;579:1951–1960.
10. Borges TJ, Murshid A, Thériault J, Calderwood SK. Molecular chaperone receptors: an update. *Methods Mol Biol.* 2023;2693:193–208.
11. Varki A, Angata T. Siglecs - the major subfamily of I-type lectins. *Glycobiology.* 2006;16:1R-27R.
12. Crocker PR, Paulson JC, Varki A. Siglecs and their roles in the immune system. *Nat Rev Immunol.* 2007;7:255–266.
13. Delneste Y, Magistrelli G, Gauchat JF, et al. Involvement of LOX-1 in dendritic cell-mediated antigen cross-presentation. *Immunity.* 2002;17:353–362.
14. Park H, Adsit FG, Boyington JC. The 1.4 angstrom crystal structure of the human oxidized low density lipoprotein receptor lox-1. *J Biol Chem.* 2005;280:13593–13599.
15. Falconi M, Ciccone S, D'Arrigo P, et al. Design of a novel LOX-1 receptor antagonist mimicking the natural substrate. *Biochem Biophys Res Commun.* 2013;438:340–345.
16. Biocca S, Iacovelli F, Matarazzo S, et al. Molecular mechanism of statin-mediated LOX-1 inhibition. *Cell Cycle.* 2015;14:1583–1595.
17. Kozakov D, Hall DR, Xia B, et al. The ClusPro web server for protein-protein docking. *Nat Protoc.* 2017;12:255–278.
18. Murshid A, Gong J, Prince T, Borges TJ, Calderwood SK. Scavenger receptor SREC-I mediated entry of TLR4 into lipid microdomains and triggered inflammatory cytokine release in RAW 2647 cells upon LPS activation. *PLoS One.* 2015;10:1–24.
19. Mehta JL, Sanada N, Hu CP, et al. Deletion of LOX-1 reduces atherogenesis in LDLR knockout mice fed high cholesterol diet. *Circ Res.* 2007;100:1634–1642.
20. Boyd CR, Orr SJ, Spence S, et al. Siglec-E is up-regulated and phosphorylated following lipopolysaccharide stimulation in order to limit TLR-driven cytokine production. *J Immunol.* 2009;183:7703–7709.
21. Mentrup T, Cabrera-Cabrera F, Schröder B. Proteolytic regulation of the lectin-like oxidized lipoprotein receptor LOX-1. *Front Cardiovasc Med.* 2021;7:594441.
22. Yu Z, Maoui M, Wu L, Banville D, Shen S. mSiglec-E, a novel mouse CD33-related siglec (sialic acid-binding immunoglobulin-like lectin) that recruits Src homology 2 (SH2)-domain-containing protein tyrosine phosphatases SHP-1 and SHP-2. *Biochem J.* 2001;353:483–492.
23. Chen GY, Brown NK, Wu W, et al. Broad and direct interaction between TLR and Siglec families of pattern recognition receptors and its regulation by Neu1. *eLife.* 2014;3:e04066.
24. Hato T, Dagher PC. How the innate immune system senses trouble and causes trouble. *Clin J Am Soc Nephrol.* 2015;10:1459–1469.
25. Rock KL, Lai JJ, Kono H. Innate and adaptive immune responses to cell death. *Immunol Rev.* 2011;243:191–205.
26. Medzhitov R. Approaching the asymptote: 20 years later. *Immunity.* 2009;30:766–775.
27. Thériault JR, Adachi H, Calderwood SK. Role of scavenger receptors in the binding and internalization of heat shock protein 70. *J Immunol.* 2006;177:8604–8611.
28. Enomoto Y, Bharti A, Khaleque AA, et al. Enhanced immunogenicity of heat shock protein 70 peptide complexes from dendritic cell-tumor fusion cells. *J Immunol.* 2006;177:5946–5955.
29. Gong J, Zhu B, Murshid A, et al. T cell activation by heat shock protein 70 vaccine requires TLR signaling and scavenger receptor expressed by endothelial cells-1. *J Immunol.* 2009;183:3092–3098.
30. Gong J, Zhang Y, Durfee J, et al. A heat shock protein 70-based vaccine with enhanced immunogenicity for clinical use. *J Immunol.* 2010;184:488–496.
31. Hutzler S, Özgör L, Naito-Matsui Y, et al. The ligand-binding domain of Siglec-G is crucial for its selective inhibitory function on B1 cells. *J Immunol.* 2014;192:5406–5414.
32. Muller J, Obermeier I, Wohner M, et al. CD22 ligand-binding and signaling domains reciprocally regulate B-cell Ca²⁺ signaling. *Proc Natl Acad Sci USA.* 2013;110:12402–12407.
33. MacAuley MS, Crocker PR, Paulson JC. Siglec-mediated regulation of immune cell function in disease. *Nat Rev Immunol.* 2014;14:653–666.
34. Rumpret M, Drylewicz J, Ackermans LJE, Borghans JAM, Medzhitov R, Meyaard L. Functional categories of immune inhibitory receptors. *Nat Rev Immunol.* 2020;20:771–780.
35. Vega VL, Rodriguez-Silva M, Frey T, et al. Hsp70 translocates into the plasma membrane after stress and is released into the extracellular environment in a membrane-associated form that activates macrophages. *J Immunol.* 2008;180:4299–4307.
36. De Maio A. Extracellular heat shock proteins, cellular export vesicles, and the Stress Observation System: a form of communication during injury, infection, and cell damage: it is never known how far a controversial finding will go! Dedicated to Ferruccio Ritossa. *Cell Stress Chaperones.* 2011;16:235–249.
37. De Maio A, Hightower LE. Heat shock proteins and the biogenesis of cellular membranes. *Cell Stress Chaperones.* 2021;26:15–18.
38. Chalmin F, Ladoire S, Mignot G, et al. Membrane-associated Hsp72 from tumor-derived exosomes mediates STAT3-dependent immunosuppressive function of mouse and human myeloid-derived suppressor cells. *J Clin Invest.* 2010;120:457–471.
39. Hsu Y-W, Hsu F-F, Chiang M-T, et al. Siglec-E retards atherosclerosis by inhibiting CD36-mediated foam cell formation. *J Biomed Sci.* 2021;28:5.
40. Fessler MB, Parks JS. Intracellular lipid flux and membrane microdomains as organizing principles in inflammatory cell signaling. *J Immunol.* 2011;187:1529–1535.
41. Sunshine H, Iruela-Arispe ML. Membrane lipids and cell signaling. *Curr Opin Lipidol.* 2017;28:408–413.
42. Ohki I, Ishigaki T, Oyama T, et al. Crystal structure of human lectin-like, oxidized low-density lipoprotein receptor 1 ligand binding domain and its ligand recognition mode to OxLDL. *Structure.* 2005.

43. Ibarlucea-Benitez I, Weitzenfeld P, Smith P, Ravetch JV. Siglecs-7/9 function as inhibitory immune checkpoints in vivo and can be targeted to enhance therapeutic antitumor immunity. *Proc Natl Acad Sci USA*. 2021;118:e2107424118.
44. Siddiqui S, Schwarz F, Springer S, et al. Studies on the detection, expression, glycosylation, dimerization, and ligand binding properties of mouse Siglec-E. *J Biol Chem*. 2017;292:1029–1037.
45. Fong JJ, Tsai C-M, Saha S, Nizet V, Varki A, Bui JD. Siglec-7 engagement by GBS β -protein suppresses pyroptotic cell death of natural killer cells. *Proc Natl Acad Sci*. 2018;115:10410–10415.
46. Landig CS, Hazel A, Kellman BP, et al. Evolution of the exclusively human pathogen *Neisseria gonorrhoeae*: human-specific engagement of immunoregulatory Siglecs. *Evol Appl*. 2019;12:337–349.
47. Siddiqui SS. Non-canonical roles of Siglecs: beyond sialic acid-binding and immune cell modulation. *Mol Aspects Med*. 2023;90:101145.
48. McMillan SJ, Sharma RS, McKenzie EJ, et al. Siglec-E is a negative regulator of acute pulmonary neutrophil inflammation and suppresses CD11b b2-integrin-dependent signaling. *Blood*. 2013;121:2084–2094.
49. Uchiyama S, Sun J, Fukahori K, et al. Dual actions of group B Streptococcus capsular sialic acid provide resistance to platelet-mediated antimicrobial killing. *Proc Natl Acad Sci*. 2019;116:7465–7470.
50. Murshid A, Theriault J, Gong J, Calderwood SK. Investigating receptors for extracellular heat shock proteins. *Methods Mol Biol*. 2011;787:289–302.
51. Horie T, Inomata M, Into T, Hasegawa Y, Kitai N. Identification of OmpA-Like protein of tannerella forsythia as an O-linked glycoprotein and its binding capability to lectins. *PLoS One*. 2016;11:e0163974.
52. Hinagata JI, Kakutani M, Fujii T, et al. Oxidized LDL receptor LOX-1 is involved in neointimal hyperplasia after balloon arterial injury in a rat model. *Cardiovasc Res*. 2006;69:263–271.
53. Webb B, Sali A. Comparative protein structure modeling using MODELLER. *Curr Protoc Bioinformatics*. 2016.2016:5.6.1-5.6.32.
54. Kelley LA, Mezulis S, Yates CM, Wass MN, Sternberg MJE. The Phyre2 web portal for protein modeling, prediction and analysis. *Nat Protoc*. 2015;10:845–858.
55. Zimmermann L, Stephens A, Nam SZ, et al. A completely reimplemented MPI bioinformatics toolkit with a New HHpred server at its core. *J Mol Biol*. 2018;430:2237–2243.
56. Notredame C, Higgins DG, Heringa J. T-coffee: a novel method for fast and accurate multiple sequence alignment. *J Mol Biol*. 2000;302:205–217.
57. Benkert P, Tosatto SCE, Schomburg D. QMEAN: a comprehensive scoring function for model quality assessment. *Proteins-Struct Funct Bioinf*. 2008;71:261–277.
58. Maghrabi AHA, McGuffin LJ. ModFOLD6: an accurate web server for the global and local quality estimation of 3D protein models. *Nucleic Acids Res*. 2017;45:W416–W421.
59. McGuffin LJ, Shuid AN, Kempster R, et al. Accurate template-based modeling in CASP12 using the IntFOLD4-TS, ModFOLD6, and ReFOLD methods. *Proteins: Struct Funct Bioinf*. 2018;86 Suppl 1:335–344.
60. Pettersen EF, Goddard TD, Huang CC, et al. UCSF Chimera—a visualization system for exploratory research and analysis. *J Comput Chem*. 2004;25:1605–1612.
61. Goddard TD, Huang CC, Meng EC, et al. UCSF ChimeraX: meeting modern challenges in visualization and analysis. *Protein Sci*. 2018;27:14–25.